J Electroceram (2010) 24:69–75
DOI 10.1007/s10832-008-9442-1

Hydrothermal synthesis of $LiFePO_4$ with small particle size and its electrochemical properties

Akira Kuwahara · Shinya Suzuki · Masaru Miyayama

Received: 9 November 2007 / Accepted: 8 February 2008 / Published online: 28 February 2008

Abstract Lithium iron phosphate ($LiFePO_4$) powders were prepared by hydrothermal reactions under a nitrogen atmosphere or an air atmosphere, and the microstructure and electrochemical properties of the $LiFePO_4$ powders were investigated. The $LiFePO_4$ powder prepared under the nitrogen atmosphere ($LiFePO_4$–N_2) had a small particle size in the range of 300–500 nm, whereas the powder prepared under the air atmosphere ($LiFePO_4$–air) had a large particle size in the range of 1–5 μm. Although the Fe^{2+}/Fe^{3+} ratio was not significantly different in both $LiFePO_4$ powders, the Fe^{2+}/Fe^{3+} ratio in the precursor suspension prepared under the nitrogen atmosphere was much higher than that prepared under the air atmosphere, thereby resulting in the small particle size of the $LiFePO_4$–N_2 powder. The discharge capacity of a $LiFePO_4$–N_2 electrode was 149 mAh g^{-1} at a low current density of 10 mA g^{-1}, whereas that of a $LiFePO_4$–air electrode was 83 mAh g^{-1}. Impedance analyses indicated that the charge transfer resistances normalized to the surface area of $LiFePO_4$ particles for the $LiFePO_4$–N_2 and $LiFePO_4$–air electrodes were 4.6 and 4.8 Ω m^2, respectively. These values were not significantly different. This revealed that the factor dominating the electrochemical properties of $LiFePO_4$–N_2 and $LiFePO_4$–air powders was particle size and not crystalline lattice or Fe^{2+} concentration.

Keywords Lithium ion batteries · $LiFePO_4$ · Hydrothermal synthesis · Particle growth

A. Kuwahara (✉) · S. Suzuki · M. Miyayama
Research Center for Advanced Science and Technology,
The University of Tokyo,
4-6-1 Komaba,
Meguro, Tokyo 153-8904, Japan
e-mail: fwd2akira@crm.rcast.u-tokyo.ac.jp

1 Introduction

Energy storage devices with a high energy and a high power are being developed for use as power sources of electric and hybrid vehicles. Lithium ion batteries [1] have been applied in many portable electronic devices because of their high energy density. However, besides this high specific energy requirement, long cycle life, environmental safety and low cost are also required. Lithium iron phosphate ($LiFePO_4$) is a promising candidate cathode material for lithium ion batteries [2]. The olivine-based structure of $LiFePO_4$ consists of a polyoxyanionic framework containing LiO_6, FeO_6 octahedra and PO_4 tetrahedra [3]. $LiFePO_4$ has a large theoretical charge/discharge capacity of 170 mAh g^{-1} and a long cycle life [4]. In addition, when lithium is extracted from $LiFePO_4$, a flat potential plateau is observed owing to the existence of $LiFePO_4$ and $FePO_4$ phases. Moreover, $LiFePO_4$ is non-toxic and inexpensive. However, the electrochemical property of $LiFePO_4$ is limited by its low lithium diffusion constant (approximately 10^{-14}–10^{-16} cm^2 s^{-1}) and low electronic conductivity (approximately 10^{-9} S cm^{-1}) [2, 5]. Padhi et al. reported that the degree of lithium intercalation/deintercalation of $LiFePO_4$ is limited to approximately 0.6 Li per formula unit [6]. A low lithium diffusion constant in electrodes leads to a charge/discharge capacity loss due to lithium diffusion limitations.

Many studies have been conducted to eliminate lithium diffusion limitations in $LiFePO_4$ by reducing particle size. Yamada et al. reported that $LiFePO_4$ with a small particle size synthesized by a solid state reaction shows a large discharge capacity of 162 mAh g^{-1} [7]. A reduction in particle size leads to a reduction in lithium diffusion distance. Therefore, lithium diffusion limitations are eliminated by reducing particle size. Yamada et al. also analyzed

the oxidation state of Fe by Mössbauer spectroscopy and reported that the oxidation state of Fe is Fe^{2+} in most of $LiFePO_4$. Preventing the formation of Fe^{3+} as impurities in $LiFePO_4$ contributes to achieving a large lithium intercalation charge/discharge capacity. Kim et al. reported that $LiFePO_4$ with nanoparticles synthesized by a polyol process shows a large discharge capacity of 166 mAh g^{-1} [8]. The nanoparticles of $LiFePO_4$ showed an excellent high-rate charge/discharge performance. Yang et al. reported a hydrothermal reaction method for synthesizing $LiFePO_4$ which showed a discharge capacity of 100 mAh g^{-1} [9]. The particle sizes of $LiFePO_4$ synthesized by hydrothermal reactions are smaller than those of $LiFePO_4$ synthesized by solid-state reactions. However, its discharge capacity decreases with an increase in the amount of Fe^{3+} ions, which are produced through Fe^{2+} oxidation by dissolved oxygen in aqueous solutions. Accordingly, a synthesis method for obtaining a small particle size without inducing Fe^{3+} oxidation is required. Tajimi et al. reported the addition of polyethylene glycol to the precursor solution to obtain fine particles, and the obtained $LiFePO_4$ showed a large discharge capacity of 143 mAh g^{-1} [10]. Shiraishi et al. reported an additional heat treatment under an inert atmosphere to crystallize the amorphous phase on the surface of particles of $LiFePO_4$ synthesized by hydrothermal reactions [11]. Dokko et al. reported a hydrothermal reaction of $LiFePO_4$ under an inert atmosphere to prohibit undesirable oxidation of Fe^{2+} during a hydrothermal process, and the obtained $LiFePO_4$ showed a large discharge capacity of 150 mAh g^{-1} [12]. Hydrothermal reaction of $LiFePO_4$ under an inert atmosphere is used to obtain high-purity crystals [12–14]. Whittingham et al. reported that the temperature above 175 °C for hydrothermal synthesis of $LiFePO_4$ contributes to a decrease in iron disorder [13]. Nazar et al. controlled particle size of hydrothermally synthesized $LiFePO_4$ by selecting synthesis temperature and reactant concentrations [14]. They indicated that a high concentration of reactants leads to a large number of nucleation sites for $LiFePO_4$ and then to the formation of small particles. Accordingly, when oxygen gas is contaminated during hydrothermal synthesis, it is assumed that a decrease in Fe^{2+} concentration as the nucleation site and a change in particle size of $LiFePO_4$ are brought about. Although many researchers conducted controlling synthesis atmosphere to obtain high-purity crystals, no studies to investigate the relationship between particle size and synthesis atmosphere in hydrothermal reactions have been conducted.

In this study, hydrothermal reactions of $LiFePO_4$ under a nitrogen atmosphere were used to synthesize $LiFePO_4$ powder with a small particle size and to achieve a large discharge capacity by maintaining a low Fe^{3+} concentration. The particle size and lithium intercalation properties of the $LiFePO_4$ powder were examined, and compared with those of $LiFePO_4$ powder synthesized under an air atmosphere. The relationship between particle size and synthesis atmosphere in hydrothermal reactions was evaluated, and the mechanism of particle growth was elucidated in the hydrothermal reactions.

2 Experimental

$LiFePO_4$ was synthesized by hydrothermal reactions [7, 9, 11] under a nitrogen atmosphere. 1 M of $FeSO_4{\cdot}7H_2O$ (Wako Chemicals), 85 wt% of H_3PO_4 (Wako Chemicals), and 1 M of $LiOH{\cdot}H_2O$ (High Purity Chemicals) in the molar ratio 1.0:1.0:3.0 were dissolved in deionized water under the nitrogen atmosphere and then mixed. The Fe^{2+} concentrations in precursor suspensions were measured by adsorption spectroscopy at a wavelength of 470 nm in $FeSO_4$ solutions. Polyethylene glycol (Wako Chemicals) was added to the solution at half the volume of the solution to obtain fine particles [10]. The resulting solution and nitrogen gas were placed in a Teflon crucible of 100 ml inner volume, which was then sealed and set in a pressure-resistant container. Hydrothermal reactions were performed at 150 °C for 3 h in the nitrogen atmosphere, and the $LiFePO_4$ powder obtained was annealed in a 1% hydrogen–99% argon atmosphere at 500 °C for 1 h to crystallize amorphous phases [15]. The particle size of the $LiFePO_4$ powder was determined by scanning electron microscopy (Hitachi, S-4500). The specific surface area of the $LiFePO_4$ powder was evaluated by nitrogen adsorption-desorption measurement (Micromeritics, TriStar3000). The crystal structure of the $LiFePO_4$ powder was evaluated by X-ray diffraction analysis using Cu Kα radiation (Bruker AXS, D8 diffractometer). The X-ray diffraction data were refined by the Rietveld method at angle intervals from 15° to 105° (2θ) in 0.02° (2θ) steps. The Rietveld refinement was carried out using the RIETAN program [16] in the space group *Pnma*. Atomic positional parameters and isotropic thermal factors were refined. The valence states of Fe in the $LiFePO_4$ powder were analyzed by Mössbauer spectroscopy, which was performed in the transmission mode using ^{57}Co γ-ray sources at room temperature. Doppler velocity was calibrated using pure Fe as a standard.

$LiFePO_4$ powder for comparison was synthesized by hydrothermal synthesis in an air atmosphere. The synthesis conditions except for the atmosphere during mixture preparation and hydrothermal reactions were the same.

The electrodes for electrochemical measurement were fabricated by pressing a mixture of $LiFePO_4$ powder, acetylene black (Denki Kagaku Kogyo) and Teflon binder (Du Pont) onto a nickel mesh. The weight ratio of $LiFePO_4$, acetylene black and Teflon was 45:45:10. The mass loading of $LiFePO_4$ in the electrodes was approximately 1×10^{-2} g

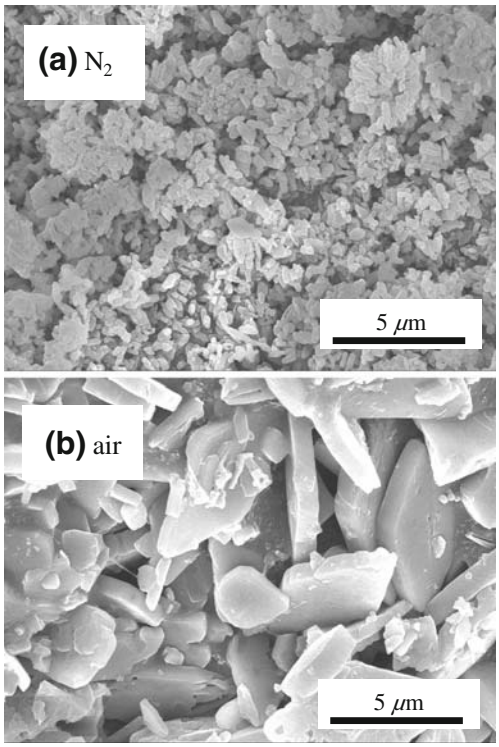

Fig. 1 Scanning electron microscopic images of various $LiFePO_4$ powders. (**a**) $LiFePO_4$-N_2, (**b**) $LiFePO_4$–air

cm^{-2}. Electrochemical measurement was performed using a three-electrode cell with a counter-electrode and a reference-electrode both made of lithium. The electrolyte used was 1 M $LiClO_4$/PC (Kishida Chemical). The cells were assembled in an argon-filled glove box at room temperature. Cyclic voltammetry was carried out at a sweep rate of 0.1 mV s^{-1}, and galvanostatic charge and discharge measurements were carried out in the current density range of 10–2,000 mA g^{-1}. All measurements were performed in the voltage range of 2.5–4.3 V with a potentiostat/galvanostat (Hokuto Denko, HAG-5001) at room temperature. Electrochemical impedance measurement was carried out in the frequency range of 20 kHz–10 mHz with ac amplitude of 20 mV at a potential of 3.45 V.

3 Results and discussion

Figure 1(a) and (b) show scanning electron microscope images of the $LiFePO_4$ powders hydrothermally synthesized in the nitrogen ($LiFePO_4$–N_2) and air ($LiFePO_4$–air) atmospheres followed by annealing in the 1% hydrogen–99% argon atmosphere, respectively. The particle size of the $LiFePO_4$–N_2 powder was in the range of 300–500 nm, and that of the $LiFePO_4$–air powder was in the range of 1–5 μm. The particle size of the $LiFePO_4$–N_2 powder was smaller than that of the $LiFePO_4$–air powder. The Brunauer–Emmett–Teller (BET) surface areas of the $LiFePO_4$–N_2 powder and $LiFePO_4$–air powder were 4.5–4.7 m^2 g^{-1} and 2.4–2.5 m^2 g^{-1}, respectively. The surface area of the $LiFePO_4$–N_2 powder was larger than that of the $LiFePO_4$–air powder. A decrease in particle size leads to a reduction in lithium diffusion distance and an increase in specific surface area. Thus, a large charge/discharge capacity is expected in $LiFePO_4$–N_2 with a small particle size.

Figure 2(a) and (b) show the measured X-ray diffraction patterns and the result of Rietveld refinement using the program RIETAN [16] for the $LiFePO_4$-N_2 powder and the $LiFePO_4$–air powder, respectively. All the peak positions of these $LiFePO_4$ powders were consistent with the calculated peak positions of $LiFePO_4$ indicated by the vertical marks. Therefore, no impurities were detected by X-ray diffraction analysis in both $LiFePO_4$ powders. The cell parameters obtained by Rietveld refinement for the $LiFePO_4$–N_2

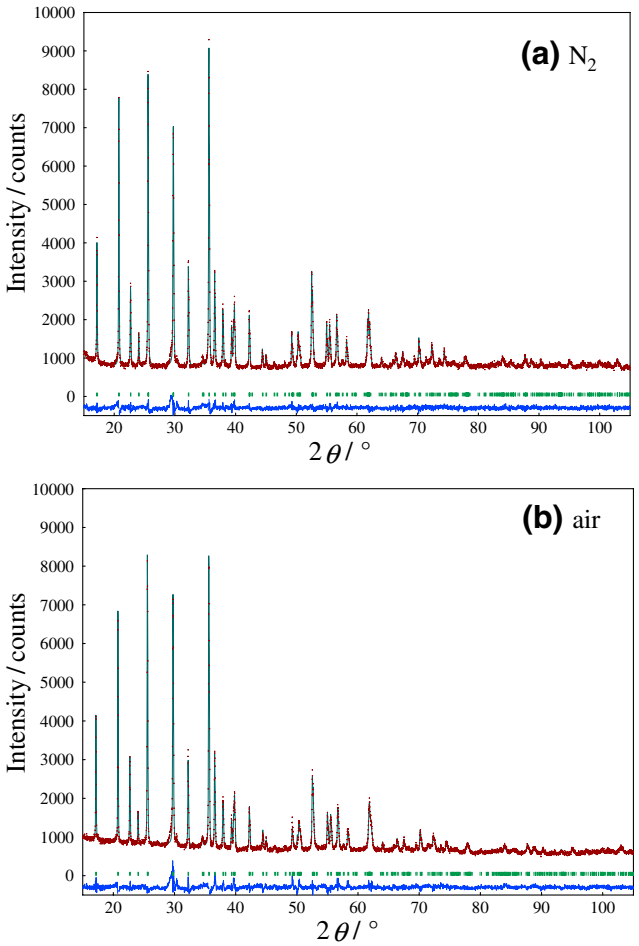

Fig. 2 X-ray diffraction patterns of various $LiFePO_4$ powders. (**a**) $LiFePO_4$–N_2, (**b**) $LiFePO_4$–air. The measured and calculated patterns are represented by the *dotted* and *solid lines*, respectively. The vertical marks in the middle show the positions calculated for Bragg reflections. The trace at the bottom is a plot of the difference between the calculated and measured intensities

powder were a=1.03280(5) nm, b=0.60040(3) nm and c=0.46936(2) nm, and the cell volume was 0.29105(2) nm^3. R_{wp} and S were 4.50% and 1.39, respectively. The cell parameters for the $LiFePO_4$–air powder were a=1.03264(9) nm, b=0.60013(5) nm and c=0.46980(4) nm, and the cell volume was 0.29114(4) nm^3. R_{wp} and S were 5.69% and 1.64, respectively. These cell parameters were almost the same and were in good agreement with previous results of $LiFePO_4$ synthesized by hydrothermal reactions [13].

Figure 3(a) and (b) show the room-temperature Mössbauer spectra of the $LiFePO_4$–N_2 powder and the $LiFePO_4$–air powder, respectively. Both spectra separated into two doublets. The spectrum of the $LiFePO_4$–N_2 powder showed an isomer shift (IS)=1.22 mm s^{-1} and a quadrupole splitting (QS)=2.96 mm s^{-1} in the major symmetric doublet. In the minor doublet, IS=0.45 mm s^{-1} and QS=0.63 mm s^{-1} were obtained. The areas of the major and minor doublets were 91% and 9% of the total area, respectively. The major doublet is typical of octahedral Fe^{2+} ions in ionic compounds [7]. Therefore, Fe^{2+} ions in the $LiFePO_4$ powders existed in an abundance ratio of 91%. Fe^{3+} ions of 9% are assumed to be formed by the reaction with residual oxygen in deionized water or already exist in $FeSO_4$ although the $LiFePO_4$–N_2 powder was synthesized under the nitrogen atmosphere. The spectrum of the $LiFePO_4$–air powder showed IS=1.22 mm s^{-1} and QS=2.95 mm s^{-1} in the major symmetric doublet. In the minor doublet, IS=0.48 mm s^{-1} and QS=0.67 mm s^{-1} were obtained. The areas of the major and minor doublets were 90% and 10% of the total area, respectively. Therefore, Fe^{2+} ions in the $LiFePO_4$ powders existed in an abundance ratio of 90%. The Fe^{2+} amounts in the $LiFePO_4$–N_2 and $LiFePO_4$–air powders were not significantly different, although there is a slight deviation. No impurity phase with Fe^{3+} ions in these $LiFePO_4$ powders was detected by X-ray diffraction analysis. It is assumed that impurities are amorphous or exist as nanoparticles [7].

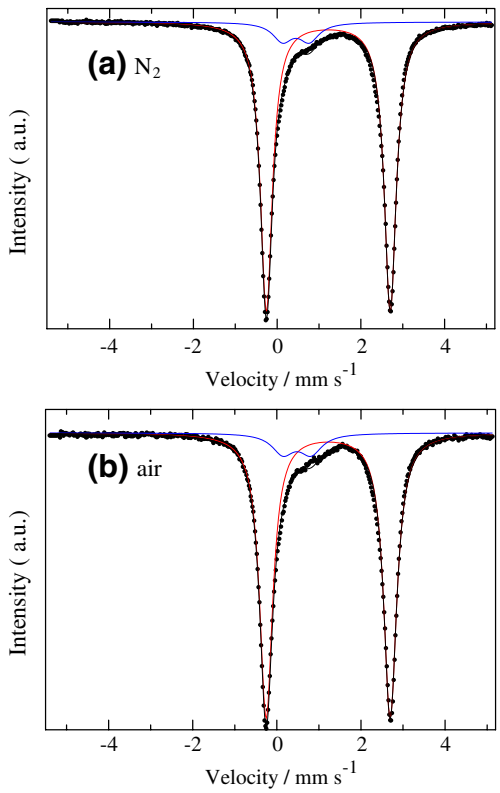

Fig. 3 Mössbauer spectra of various $LiFePO_4$ powders. (**a**) $LiFePO_4$–N_2, (**b**) $LiFePO_4$–air. The measured pattern is represented by the *dotted line*. The calculated patterns are represented by the *solid lines*

The reaction equations in this hydrothermal condition are described in two step reactions. The reaction formula for the first reaction, that is the generation of the suspension solution with $Fe(OH)_2$, can be written as

$$2LiOH + FeSO_4 \rightarrow +Fe(OH)_2 + Li_2SO_4. \quad (1)$$

The reaction formula for the second reaction, that is the formation of $LiFePO_4$ during hydrothermal synthesis, can be written as

$$LiOH + Fe(OH)_2 + H_3PO_4 \rightarrow LiFePO_4 + 3H_2O. \quad (2)$$

In the first reaction step, the color of the precursor suspension for the $LiFePO_4$–N_2 powder was greenish white, and the major suspended solids were $Fe(OH)_2$. The color of the precursor suspension for the $LiFePO_4$–air powder was dark green, and the suspended solids were a mixture of $Fe(OH)_2$ and $Fe(OH)_3$. Fe^{2+} concentrations in the $LiFePO_4$–N_2 and the $LiFePO_4$–air precursor suspensions were 83% and 28%, respectively. In the second reaction step, $Fe(OH)_2$ solids function as the cores of $LiFePO_4$ crystals. In the precursor solution of $LiFePO_4$–air, $Fe(OH)_3$ solids as impurities are produced through oxidation of Fe^{2+} ions due to oxygen dissolved in aqueous solutions. Therefore, the amount of $Fe(OH)_2$, crystal nucleation cores, in the $LiFePO_4$–air precursor solution is less than that in the $LiFePO_4$–N_2 precursor solution. This change is consistent with the result of Nazar et al. [14], indicating the formation of small particles by increased reactant concentrations. In the hydrothermally synthesized $LiFePO_4$, the Fe^{2+} concentrations in the $LiFePO_4$–N_2 powder and the $LiFePO_4$–air powder were 91% and 90%, respectively. The Fe^{2+} amounts in the $LiFePO_4$–N_2 powder and the $LiFePO_4$–air powder were not significantly different although hydrothermal reactions were conducted in different atmospheres. It is assumed that polyethylene glycol performed as a reduction agent [17, 18] and the reduction of Fe^{3+} components occurred during hydrothermal reactions. When the formation of $LiFePO_4$ occurs with Fe^{2+} reduced by polyethylene glycol in hydrothermal reactions (Eq. 2), the formation of $LiFePO_4$ occurs

dominantly on the surface of $LiFePO_4$ particles already present. Therefore, the particle growth of the $LiFePO_4$–air is enhanced because the amount of crystal nucleation cores is small and the amount of Fe^{2+} reduced in the hydrothermal reactions is large.

Figure 4 shows the cyclic voltammograms of the $LiFePO_4$–N_2 and $LiFePO_4$–air electrodes at a sweep rate of 0.1 mV s^{-1}. Each electrode exhibited reversible reduction and oxidation. The anodic/cathodic peaks centered at an equilibrium potential of 3.45 V were attributed to the lithium intercalation/deintercalation of $LiFePO_4$. However, the degree of peak shift from the equilibrium potential differed between these $LiFePO_4$ electrodes. The difference between the peak potentials of the $LiFePO_4$–N_2 electrode was approximately 250 mV, and that of the $LiFePO_4$–air electrode was approximately 275 mV. When lithium intercalation and deintercalation occur rapidly and the electronic resistance of the electrode is sufficiently small, the difference between the peak potentials becomes smaller and the peaks become sharper. The electrical resistances of these $LiFePO_4$ electrodes were sufficiently small because of the high carbon contents of the electrodes. Therefore, it is suggested that lithium intercalation and deintercalation occurred rapidly in the $LiFePO_4$–N_2 electrode. The large surface area of the $LiFePO_4$–N_2 electrode is responsible for the increase in apparent lithium intercalation and deintercalation rate.

Figure 5(a) shows the charge and discharge curves for the $LiFePO_4$–N_2 electrode at 10 mA g^{-1} and the discharge curves in the current density range of 10–1,000 mA g^{-1}. The charge and discharge capacity per unit weight of $LiFePO_4$ was 149 and 150 mAh g^{-1} at a low current density of 10 mA g^{-1}. The $LiFePO_4$ electrode showed reversible capacities under charge and discharge, and a flat discharge potential plateau was observed at approximately 3.4 V. This discharge capacity was approximately 90% of the theoretical capacity of $LiFePO_4$. Discharge capacity losses

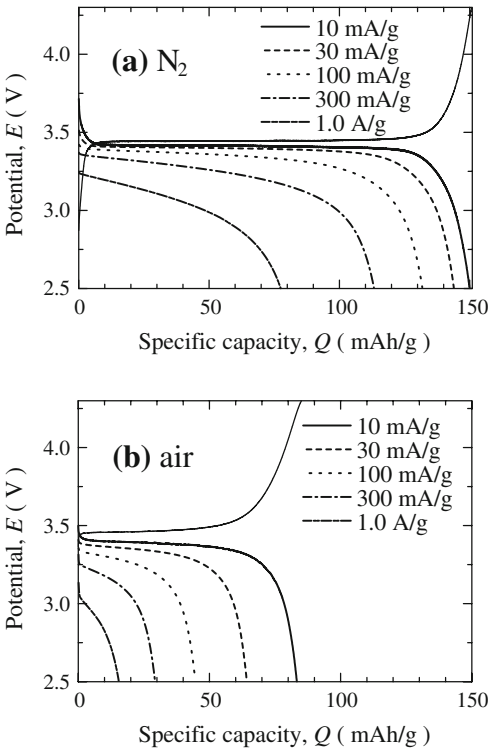

Fig. 5 Charge and discharge curves for various $LiFePO_4$ electrodes. (**a**) $LiFePO_4$–N_2, (**b**) $LiFePO_4$–air. The current density range was 10–1,000 mA g^{-1}

occurred and flat discharge potential plateaus disappeared with increasing current density. The discharge capacities of the $LiFePO_4$ electrode were 131 mAh g^{-1} at 100 mA g^{-1} and 77 mAh g^{-1} at 1000 mA g^{-1}.

Figure 5(b) shows the charge and discharge curves for the $LiFePO_4$–air electrode at 10 mA g^{-1} and the discharge curves in the current density range of 10–1,000 mA g^{-1}. The charge and discharge capacity of the $LiFePO_4$ electrode was 83 and 85 mAh g^{-1} at a low current density of 10 mA g^{-1}. The $LiFePO_4$ electrode showed reversible capacities under charge and discharge, and a flat discharge

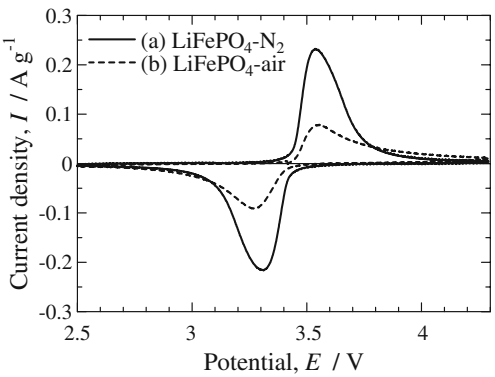

Fig. 4 Cyclic voltammograms of various $LiFePO_4$ electrodes. (a) Solid line representing $LiFePO_4$–N_2, (b) *dashed line* representing $LiFePO_4$–air. The sweep rate was 0.1 mV s^{-1}

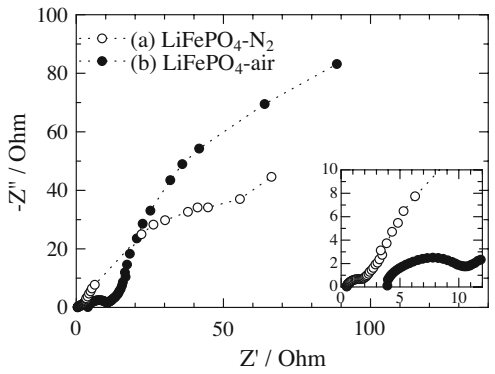

Fig. 6 Impedance plots of various $LiFePO_4$ electrodes. (a) *White circles* representing $LiFePO_4$–N_2, (b) *black circles* representing $LiFePO_4$–air. The potential voltage was 3.45 V and the ac amplitude was 20 mV

potential plateau was observed at approximately 3.4 V. Discharge capacity decreased markedly with increasing current density, and reached 44 at 100 mA g^{-1} and 15 at 1,000 mA g^{-1}. At a low current density of 10 mA g^{-1}, the discharge capacity of the $LiFePO_4$–air electrode was much smaller than that of the $LiFePO_4$–N_2 electrode. The small discharge capacity at the low current density of the $LiFePO_4$–air electrode was not consistent with the Fe^{2+} ratio of 90% for $LiFePO_4$ although the discharge capacity of the $LiFePO_4$–N_2 electrode was consistent with the Fe^{2+} ratio for $LiFePO_4$. This small discharge capacity of he $LiFePO_4$–air electrode is caused by the slow lithium intercalation and deintercalation rate due to the small surface area of the $LiFePO_4$–air electrode and by a long lithium diffusion distance in $LiFePO_4$ due to the large particle size. In the $LiFePO_4$–air electrode, the current density of 10 mA g^{-1} is not sufficiently low for performing the electrochemical lithium deintercalation reaction completely.

Figure 6 shows the impedance plots for these $LiFePO_4$ electrodes at a potential of 3.45 V. The spectra indicated a combination of two semicircles in the high and intermediate frequency ranges. A Warburg region, assigned to the diffusional transport of intercalated ions in cathode materials, appears at very low frequencies. However, no Warburg region was observed in the measured frequency region. The diameter of a high-frequency semicircle was assigned to an electrical resistance of the electrode and that of an intermediate-frequency semicircle was assigned to the charge transfer resistance between an electrolyte and active materials [19, 20]. The electrical and charge transfer resistances of the $LiFePO_4$–N_2 electrode were 1.9 and 1.0×10^2 Ω, respectively. The electrical and charge transfer resistances of the $LiFePO_4$–air electrode were 8.4 and 1.9×10^2 Ω, respectively. In these $LiFePO_4$ electrodes, the dominant resistance component was the charge transfer resistance. The charge transfer resistance of the $LiFePO_4$–N_2 electrode was much lower than that of the $LiFePO_4$–air electrode. The result was consistent with the difference between the peak potentials in the cyclic voltammograms shown in Fig. 4. The charge transfer reactions occur at the interface between $LiFePO_4$ particle surfaces and electrolytes. The area specific resistances, (the charge transfer resistance normalized to the surface area of $LiFePO_4$ particles), were estimated to be 4.6 Ω m^2 for the $LiFePO_4$–N_2 electrode and 4.8 Ω m^2 for the $LiFePO_4$–air electrode. These area specific resistances were almost the same, indicating that the surface reaction resistances per unit area are not significantly different for the $LiFePO_4$–N_2 and $LiFePO_4$–air electrodes. This revealed that the factor dominating the electrochemical properties of the $LiFePO_4$–N_2 and $LiFePO_4$–air powders was particle size and not the crystalline lattice or Fe^{2+} concentration.

4 Conclusions

$LiFePO_4$ powder with a small particle size was synthesized by hydrothermal reactions under nitrogen atmosphere. The $LiFePO_4$ powder prepared under the nitrogen atmosphere ($LiFePO_4$–N_2) had a small particle size in the range of 300–500 nm, whereas the particle size of the $LiFePO_4$ powder prepared under the air atmosphere ($LiFePO_4$–air) was in the range of 1–5 μm. The Fe^{2+} concentrations of the $LiFePO_4$ powders were as high as approximately 90% and were not significantly different. However, the Fe^{2+} concentration in the precursor suspension of the $LiFePO_4$–N_2 powder was 83% (much higher than 28% in the case of the $LiFePO_4$–air powder). It was suggested that a large amount of crystal nucleation cores and a low Fe^{3+} concentration in the precursor suspension are required to obtain small particles of $LiFePO_4$ in the hydrothermal synthesis. The discharge capacity of the $LiFePO_4$–N_2 electrode was 149 mAh g^{-1} at a low current density of 10 mA g^{-1}, whereas that of the $LiFePO_4$–air electrode was 83 mAh g^{-1}. The large discharge capacity of the $LiFePO_4$–N_2 electrode is attributed to the small $LiFePO_4$ particles with a large surface area, leading to the elimination of lithium diffusion limitations and the decrease in apparent charge transfer resistance. Impedance analysis indicated that the charge transfer resistances normalized to the surface area of $LiFePO_4$ particles were not significantly different for the $LiFePO_4$–N_2 and $LiFePO_4$–air electrodes. This revealed that the factor dominating the electrochemical properties of the $LiFePO_4$–N_2 and $LiFePO_4$–air powders was particle size and not the crystalline lattice or Fe^{2+} concentration.

References

1. R.J. Brodd, K.R. Bullock, R.A. Leising, R.L. Middaugh, J.R. Miller, E. Takeuchi, J. Electrochem. Soc. **151**, K1 (2004)
2. M.S. Whittingham, Chem. Rev. **104**, 4271 (2004)
3. V.A. Streltsov, E.L. Belokoneva, V.G. Tsirelson, N. Hansen, Acta Cryst. **B49**, 147 (1993)
4. A.K. Padhi, K.S. Nanjundaswamy, C. Masquelier, S. Okada, J.B. Goodenough, J. Electrochem. Soc. **144**, 1609 (1997)
5. P.P. Prosini, M. Lisi, D. Zane, M. Pasquali, Solid State Ion. **148**, 45 (2002)
6. A.K. Padhi, K.S. Nanjundaswamy, J.B. Goodenough, J. Electrochem. Soc. **144**, 1188 (1997)
7. A. Yamada, S.C. Chung, K. Hinokuma, J. Electrochem. Soc. **148**, A224 (2001)
8. D.H. Kim, J. Kim, Electrochem. Solid-State Lett. **9**, A439 (2006)
9. S. Yang, P.Y. Zavalij, M.S. Whittingham, Electrochem. Commun. **3**, 505 (2001)
10. S. Tajima, Y. Ikeda, K. Uematsu, K. Toda, M. Sato, Solid State Ion. **175**, 287 (2004)
11. K. Shiraishi, K. Dokko, K. Kanemura, J. Power Sources **146**, 555 (2005)
12. K. Dokko, S. Koizumi, K. shiraishi, K. Kanemura, J. Power Sources **165**, 656 (2007)

13. J. Chen, M.S. Whittingham, Electrochem. Commun. **8**, 855 (2006)
14. B. Ellis, W.H. Kan, W.R.M. Makahnouk, F. Nazar, J. Mater. Chem. **17**, 3248 (2007)
15. K. Dokko, K. Shiraishi, K. Kanemura, J. Electrochem. Soc. **152**, A2199 (2005)
16. F. Izumi, T. Ikeda, Mater. Sci. Forum **198–203**, 321 (2000)
17. D. Larcher, R. Patrice, J. Solid State Chem. **154**, 405 (2000)
18. L. Qiu, V.G. Pol, J.C. Moreno, A. Gedanken, Ultrason. Sonochem. **12**, 243 (2005)
19. D. Aurbach, M.D. Levi, E. Levi, H. Teller, B. Markovsky, G. Salitra, U. Heider, L. Heider, J. Electrochem. Soc. **145**, 3024 (1998)
20. M.D. Levi, G. Salitra, B. Markovsky, H. Teller, D. Aubach, J. Electrochem. Soc. **146**, 1279 (1999)